Acta Cryst. (1973). **B29**, 2171

The Low-Temperature Phase Transition of Sodium Niobate and the Structure of the Low-Temperature Phase, *N*

BY C. N. W. DARLINGTON* AND HELEN D. MEGAW

Crystallographic Laboratory, Cavendish Laboratory, Cambridge, England

(*Received* 15 *January* 1973; *accepted* 6 *March* 1973)

Sodium niobate undergoes an antiferroelectric–ferroelectric transition ($P \rightleftarrows N$) at temperatures below about -110°C. The ferroelectric low-temperature phase (N) is rhombohedral, with space group $R3c$. Though a perovskite structure, it is isostructural with $LiNbO_3$. Using pseudocubic axes of reference, $a = 2 \times 3{\cdot}9083$ (5) Å, $\alpha = 89°13$ (1)′ at -150°C. The NbO_6 octahedra remain nearly regular, but are tilted about the triad axis; displacements of Nb atoms from the centres of octahedra are parallel to this axis. The temperature dependence of the lattice parameters of both phases, N and P, below room temperature is reported, and also that of the magnitude of the Nb displacement in the antiferroelectric phase P. Experimental details of the low-temperature work are given. Evidence used in the structure determination comes from the juxtaposition of high-angle reflexions from twin components in phase N, and the orientation of domains of phase N relative to the parent phase P. The transformation is more rapid and more complete if the parent crystal is single-domain; if it is twinned, both phases coexist for long periods down to the lowest temperatures studied. The relation of the structure to that of other niobates is discussed, and some general principles are put forward from which the occurrence of different structures and the transitions between them can be understood.

1. Introduction

1.1. *The aristotype and hettotypes*

This paper describes the behaviour of sodium niobate, $NaNbO_3$ between 77°K and room temperature.

$NaNbO_3$ above 640°C has the ideal perovskite structure with space group $Pm3m$. Below this temperature a large number of displacive transitions take place (see for example Lefkowitz, Łukaszewicz & Megaw, referred to hereafter as LŁM, 1966). The phase stable at room temperature satisfies the criteria for antiferroelectricity (see Megaw, 1957), and, following LŁM (1966), we shall call this phase P.

At temperatures below about -110°C a new phase begins to appear which is ferroelectric (Cross & Nicholson, 1955). We shall call this phase N.

It is desirable to define axes of reference which can be used for all phases. The ideal perovskite structure, the aristotype, has a cubic unit cell of side about 4 Å. In the hettotypes to be considered, this cube, distorted, becomes the subcell, with sides a', b', c' which are not necessarily equal, and angles α, β, γ which are not necessarily 90°. It is convenient to continue to use pseudocubic axes of reference as standard practice, and this we shall do throughout, writing

$$a_{pc} = m_1 a'$$
$$b_{pc} = m_2 b'$$
$$c_{pc} = m_3 c'$$

where the m_i are integral. Later, it will be necessary to define the sense of these axes, a point which needs no special attention when only one phase is being considered, but which becomes important if confusion is to be avoided when, as here, we are dealing with changes of orientation in phase transitions.

For some purposes, however, we shall find it convenient to use other axes of reference. These will be introduced at the appropriate points below.

1.2. *Phase P*

Phase P has the following pseudocubic unit cell at room temperature

$$a_{pc} = c_{pc} = 2 \times (3{\cdot}9150 \pm 0{\cdot}0002)\ \text{Å}$$
$$b_{pc} = 4 \times (3{\cdot}8798 \pm 0{\cdot}0002)\ \text{Å}$$
$$\alpha = \gamma = 90°$$
$$\beta = 90°40' \pm 0{\cdot}3'.$$

The fact that $\beta - \pi/2$ is positive follows from a deliberate choice of sense of the a and c axes, to accord with the familiar convention for monoclinic structures. The projection of this unit cell down $[010]_{pc}$ is a rhombus, and therefore we may choose axes consistent with the true orthorhombic symmetry. Following the original choice by Vousden, a_0 is taken as parallel to $[10\bar{1}]_{pc}$, giving

$$a_0 = a_{pc} \cdot \sin \beta/2$$
$$b_0 = b_{pc}$$
$$c_0 = a_{pc} \cdot \cos \beta/2\ .$$

Sakowski-Cowley, Łukaszewicz & Megaw (referred to hereafter as SŁM) (1969) have reported the structure of this phase, which has space group *Pbma*. The niobium atoms are surrounded by approximately regular oxygen octahedra which are tilted relative to each other by 8° about [010] and $9\frac{1}{2}$° about $[10\bar{1}]_{pc}$. Taking the

* Present address: Department of Physics, University of Birmingham, Birmingham B15 2TT, England.

geometrical centre of the octahedron as reference point, each niobium atom is displaced by about 0·13 Å along a direction inclined by 16° to $[10\bar{1}]_{pc}$, almost exactly perpendicular to [010]. Applying the symmetry elements of the space group, we generate the Nb displacement sequence shown in Fig. 1.

1.3. *Phase N*

For phase *N*, Cross & Nicholson (1955) measured a reversible spontaneous polarization in what had been the *y* direction of phase *P*, but could not detect any moment in directions perpendicular to this. They concluded that 'the ferroelectric properties are most likely produced by an additional ferroelectric displacement of the ions in a direction perpendicular to the (010) plane'.

The structure determination of phase *N*, reported below, shows that the structure falls into the category of rhombohedral ferroelectric with polarization along $[111]_{pc}$, and that the crystal twins in passing from phase *P* to *N*, giving the macroscopic polarization scheme observed by Cross & Nicholson.

2. Experimental work

2.1. *The low-temperature apparatus*

The crystal was mounted on the goniometer head of a Weissenberg camera; the low-temperature apparatus cooled it by immersing it in a stream of cold gas collected from boiling liquid nitrogen.

The liquid nitrogen was held in a commercially available 25-litre Dewar and boiled by a controlled 48 W soldering-iron element. The cold gas left the Dewar *via* copper-nickel Dewar tubes; these were held in position by asbestos spacers mounted in the layer-line screens of the Weissenberg camera, and carried the cold gas to within 5 mm of the crystal. Ice was prevented from forming on the crystal by isolating the crystal and Dewar arm inside a cold volume provided by wrapping cellophane sheet, transparent to X-rays, round the two layer-line screens. This directed the cold gas, once it had passed over the crystal, back over itself, forming an effective sheath of dry gas. A small hole was punched in the cellophane sheet to accommodate the collimator.

A small diode, 1*S*44, located at the end of the delivery tube, was used as a temperature-sensing device. The circuit and characteristics are shown in Fig. 2. The signal from this device was constantly compared with a preselected voltage, corresponding to some chosen temperature, *via* two balanced field-effect transistors arranged in a long-tail pair. The output from this determined whether the voltage across the heater should be increased or decreased, thereby either lowering or raising the temperature at the crystal position.

The apparatus produced a cylindrical cold volume, of nearly constant temperature, about 5 mm in diameter (the diameter of the inner delivery tube) and about 10 mm in length. The temperature stability of this volume over long periods of time was better than $\pm\frac{1}{2}$°C, although the absolute temperature was known to only ±2°C. Controllable temperatures from −170°C to room temperature were obtainable. At −150°C, 0·4 l of liquid nitrogen per hr were consumed.

2.2. *Types of photographs taken*

The radiation used throughout was Cu $K\alpha$, with $\lambda(\alpha_1) = 1{\cdot}54051$, $\lambda(\alpha_2) = 1{\cdot}54433$ Å.

Lattice parameters of both phases *P* and *N* were determined from oscillation photographs taken using a Weissenberg camera. Intensity data for the structure determination of phase *N* were obtained from Weissenberg photographs taken at two temperatures. The

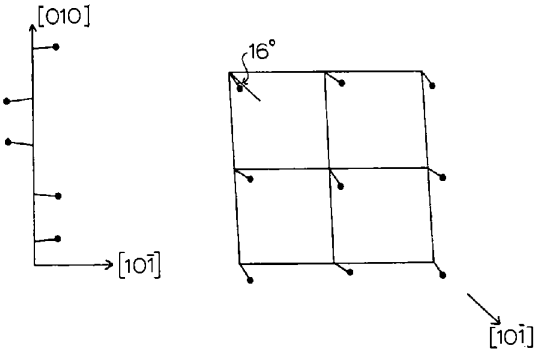

Fig. 1. Array of Nb atoms in phase *P*, (*a*) in projection on $(101)_{pc}$, (*b*) in projection on $(010)_{pc}$.

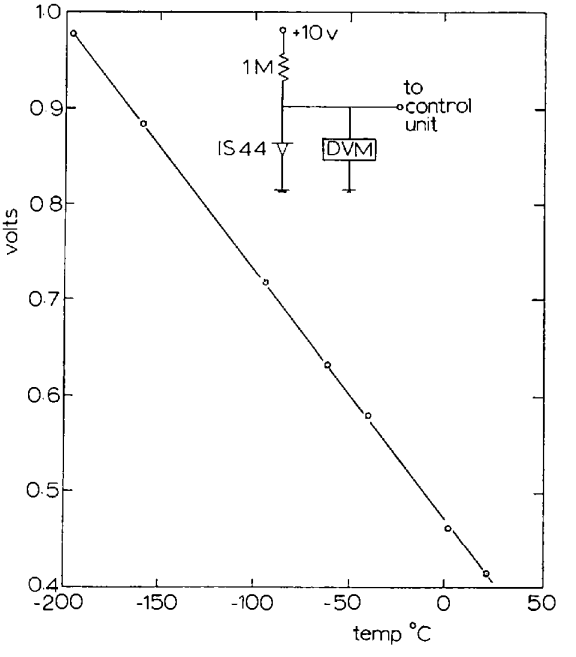

Fig. 2. Temperature-sensing circuit and characteristics.

structure was refined from data collected at −150 °C. Oscillation photographs were also used in the observation of the transformation in twinned crystals of phase *P*.

2.3. *The accurate measurement of lattice parameters using a Weissenberg camera*

(*a*) *General procedure*

Symmetrical back-reflexion photographs of single or lightly-twinned crystals were used to obtain accurate θ-values.

The cassette of the Enraf–Nonius Weissenberg camera can be easily adapted to hold the film in the van Arkel setting by removing the clips, normally used to hold the film, which run parallel to the axis of the cassette. A hole was punched in the film to accommodate the collimator. The hole was made light-tight by a simple device consisting of two thin-walled cylinders that slipped over each other, each with a flange at one end; the cylinder of smaller diameter was pushed through the hole in the film, and then, by sliding the other cylinder over the first, the black paper was held together between the two flanges. The collimator could be inserted through the inner cylinder without touching it. To avoid unnecessary bending of the film the surfaces of the flanges in contact with the black paper were ground to the natural curvature of the film when held in the cassette. The shadow of the inner flange was designed to serve as a fiducial mark on the film when it was inconvenient to record symmetrical reflexions on either side of the straight-through positions; in practice, it did not become necessary to use it in this way.

(*b*) *Random errors*

The photographs were measured with a travelling microscope made by the Cambridge Scientific Instrument Company to a National Physical Laboratory Design (Sears & Turner, 1941). By careful measurement the distances on the film were reproducible to about ±0·01 mm. This corresponds to ±1′ in θ-value. The corresponding error in *d* spacing at $\theta=80°$ is 1 part in 2×10^4.

(*c*) *Systematic errors*

Systematic error in θ-value caused by crystal misorientation was eliminated by accurately aligning the crystal by taking a series of Laue photographs. Possible film shrinkage was checked by imprinting a scale onto the film. In all cases the shrinkage was uniform and less than 4 parts in 17000, making any correction unnecessary.

The design of the Weissenberg camera makes it difficult to ensure that the oscillation axis of the crystal and the axis of the cassette coincide exactly. Any non-coincidence would cause an eccentricity error. The $\alpha_1\alpha_2$ doublet separation of high-angle reflexions is sensitive to the radius value and hence should show up an error of this type. The doublet separation of the $10,0,0_{pc}$ reflexion of phase *P* at $\theta\sim80°$, was measured on two different Weissenberg cameras. The mean value of repeated measurement gave $0{\cdot}0789_1$, $0{\cdot}0791_5$ cm for the different cameras.

From one particular reflexion, of course, one cannot determine whether the difference in the doublet separation is caused by eccentricity or whether the two cassettes have a genuinely different radius value. For the case of difference in radii, we have

$$\frac{\Delta d}{d}=-\frac{\Delta R}{R}\left(\frac{\pi}{2}-\theta\right)\cot\theta$$

where $\Delta d/d$ is the proportional difference in measured *d* spacing from the two cameras and $\Delta R/R$ is the ratio of the difference between the two measurements of the $\alpha_1\alpha_2$ doublet separation to their mean. For 10,0,0, $\Delta R/R\sim2/800$, and $\theta\sim80°$, hence

$$\left|\frac{\Delta d}{d}\right|_{\theta\sim80°}\sim1\times10^{-4}.$$

This indicates the order of magnitude of a systematic error in *d* spacing to be expected from an error in radius value.

Systematic error caused by eccentricity results in a proportional error in *d* spacing that varies with θ as $\cos^2\theta$, while for a wrongly assumed radius value the error will vary as $(\pi/2-\theta)\cot\theta$. There is little to choose between these two extrapolation functions for θ greater than about 50°, and therefore the $\cos^2\theta$ (or $\sin^2\theta$) plot was used. For all photographs it turned out that such a plot was linear within experimental error, indicating that this extrapolation eliminated the greater part of the systematic error.

To test the accuracy of the arrangement, two photographs of a single crystal of silicon were taken with Cu *K*α radiation, and the lattice parameter was found by a similar extrapolation. The values, after correction for refraction and adjustment to 25 °C were $a=5{\cdot}4304_8$, $5{\cdot}4305_1$, both ±0·0003 Å. These compare well with the value found in the I.U.Cr. lattice parameter project (Parrish, 1960) of $5{\cdot}43054\pm0{\cdot}0001_7$ Å.

2.4. *Collection of intensities*

Intensities for phase *N* from $hk0_{pc}$, $hk1_{pc}$ and $hk2_{pc}$ layers were collected at −150 °C using normal-beam Weissenberg photographs. The crystals were first cooled to −170 °C, where the transformation occurs rapidly.

The majority of the twin-related spots adjacent on the film could be resolved with care. For the even-layer photographs, the intensities were measured with a Joyce–Loebel Integrating Microdensitometer. For the *hk*1 layer, where the intensities were systematically weak, they were measured by visual comparison with a prepared intensity scale. Absorption corrections were applied to the even layers only, and Lp corrections to all reflexions. No correction because of the twinning was necessary, since symmetry-equivalent intensities produced by twin-related positions of the crystal were measured as equal within experimental error.

3. Structural parameters of phase *P*

3.1. *Lattice parameters*

For the measurement of a^*, single crystals were oscillated about $[001]_{pc}$ through an azimuthal range of $\pm 15°$ symmetrical about x^*, which allowed about ten reflexions to appear. For $l=0$,

$$\frac{1}{a^*} = \frac{\lambda}{2 \sin \theta} \left[h^2 + k^2 \left(\frac{b^*}{a^*} \right)^2 \right]^{1/2} . \qquad (1)$$

From the measured θ values, a program calculated $1/a^*$ for each reflexion for a number of different b^*/a^* values, and then determined the regression line of $1/a^*$ on $\sin^2 \theta$. According to theory, when the estimated standard deviation of $1/a^*$ at $\theta=90°$, $s(1/a^*)$, is a minimum, then the ratio b^*/a^* is such that the values of $1/a^*$ are likely to be linearly dependent on $\sin^2 \theta$. A graphical check was made on the validity of each extrapolation. The value of $s(1/a^*)$ for the pseudocubic subcell parameter at any temperature was never greater than $\pm 0{\cdot}0002$ Å.

The value of b^* obtained from the axial ratio was not used. More accurate values were obtained by oscillating the crystal about the same axis $[001]_{pc}$ through an azimuthal range symmetrical about y^*, and using a suitably modified form of (1).

The angle β was measured from type-I twinned crystals oscillated about $[010]_{pc}$. This form of twinning results in the juxtaposition on the zero layer of spots with indices $h0l_{pc}$ and $h0\bar{l}_{pc}$. In particular 806_{pc} and $80\bar{6}_{pc}$ lie close together, both with θ values of about 80°. Following LŁM (1966) we obtain

$$\beta - \frac{\pi}{2} \sim \frac{25}{24} . \Delta\theta . \cot \theta_m$$

where

$$\Delta\theta = \theta(806) - \theta(80\bar{6})$$

and

$$\theta_m = \tfrac{1}{2}[\theta(806) + \theta(80\bar{6})] .$$

The approximations give an error in β of less than $\pm 0{\cdot}1'$.

The temperature dependence of the lattice parameters in phase *P* is given in Figs. 3 and 4. The values shown in the same figures for phase *N* will be discussed in §§ 4.1 and 4.2.

3.2. *The* Nb *displacement*

The geometrical structure factor for the niobium atoms, using the orthorhombic unit cell, is

$$A = 8 \cos 2\pi \left(hu + \frac{k}{4} \right) \times \cos 2\pi \left(\frac{3k}{8} + kv \right) \cos 2\pi \left(lw + \frac{h+l}{4} \right)$$

$$B = 0 .$$

where u, v and w are the displacements from the high-symmetry position. SŁM (1969) give the following values at room temperature

$$u = 0{\cdot}0223$$
$$v = 0{\cdot}0012$$
$$w = 0{\cdot}0066 .$$

At large θ values, the intensity of the Bragg reflexions depends mainly on the niobium array; hence if we approximate by taking $v=0$ we may determine the value of u from the intensity ratio

$$\frac{I(711)_o}{I(701)_o} \sim \tfrac{1}{2} \tan^2 2\pi 7u .$$

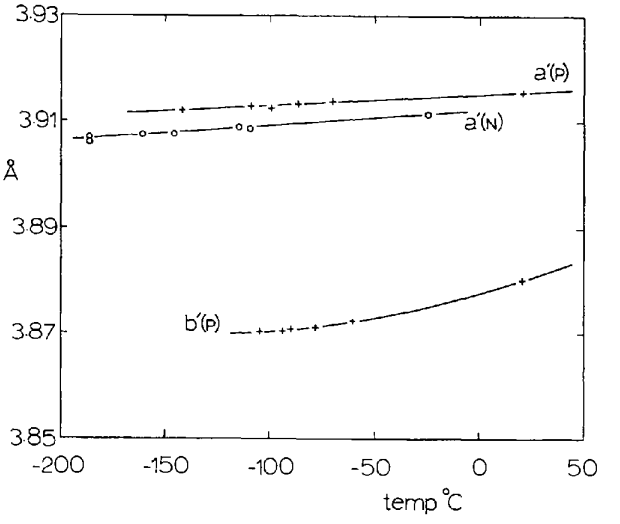

Fig. 3. Edge lengths of the pseudocubic subcell in phase *P* (crosses) and phase *N* (open circles). Note the large hysteresis.

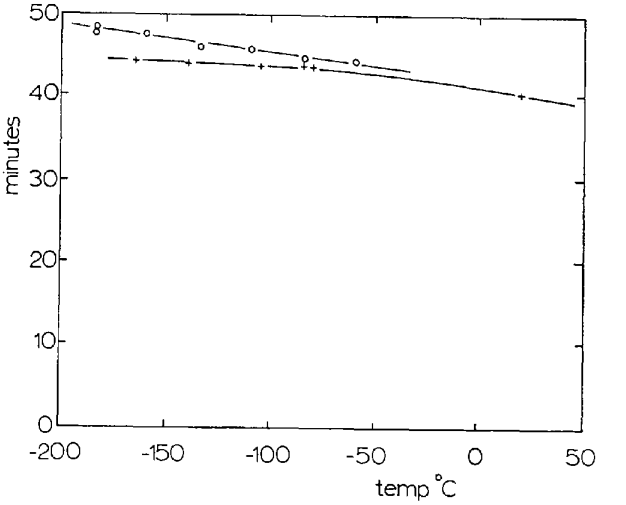

Fig. 4. Departure from 90° of the interaxial angles of the pseudocubic subcell in phase *P* (crosses give β-90°) and phase *N* (circles give 90°-α).

Both reflexions have θ values of approximately 80°.

The temperature dependence of ua_0 thus deduced is given in Fig. 5. The new values lie on a smooth curve with those measured by other authors at or above room temperature. If the room temperature relation, $w \simeq \frac{1}{3}u$, is maintained at other temperatures, the value of ua_0 is negligibly different from the total displacement of Nb in phase P.

4. Lattice relations of N and P

4.1. *Derivation of lattice of N*

The only observed reflexions in phase N are those whose indices, referred to the pseudocubic subcell, are all integers or all odd half-integers. This implies that the true cell is also pseudocubic, with each side doubled, *i.e.* with all the m_i's equal to 2; it contains 8 formula units. Hereafter, all indexing will be done with reference to this cell. Since the indices of observed reflexions are all even or all odd, the lattice is face-centred. Reflexions with even indices are exceptionally strong, those with odd indices exceptionally weak – a fact whose implications will be discussed below.

Back-reflexion photographs showed that 10,0,0, 0,10,0, and 0,0,10 all had the same interplanar spacing, *i.e.* that

$$a^* = b^* = c^*.$$

Very important information was obtained from comparison of photographs of the same crystal before and after the $P \rightarrow N$ transition. Fig. 6 shows Weissenberg photographs taken with Cu $K\alpha$ radiation. Photograph 6(*a*) was taken at room temperature and is of a single crystal of phase P oscillated about $[001]_{pc}$. Photograph 6(*b*) shows the same oscillation range taken at −110°C after the crystal had previously been cooled to −140°C for 15 min. The transformation from phase P to N is incomplete, and so spots characteristic of twinned phase N and phase P occur. This can be seen in more detail in the enlargements of high-angle regions of Fig. 6(*b*) shown in Fig. 6 (*c*) and (*d*).

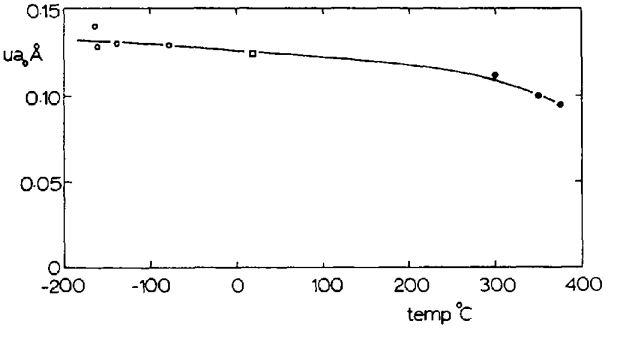

Fig. 5. Temperature dependence of the x component of the Nb displacement in phase P. Open circles, present work; square, value from the structure determination (SŁM, 1969); black circles, new unpublished measurements of Ahtee & Glazer, superceding earlier rougher measurements of Megaw (1968).

The low-temperature photograph shows that the twinning in phase N leaves b^* unique and parallel to b^* of phase P, while a^* of phase N is duplicated. This can be seen, for example, by examination of the 800 complex of spots in the enlargements 6(*c*) and 6(*d*). It follows that γ^* is no longer a right angle.

Observations over all reciprocal space concerning the separation of twin-related spots gave further information. This separation depends on the Bragg angle θ as well as on the relative orientation of twin domains, but the effect of the latter can be isolated by making comparisons within a limited range of θ. It is convenient at the first stage to continue to use for phase N the same axes of reference as have served for phase P, according to which $\theta(h0h) > \theta(h0\bar{h})$. It is then seen that $h0\bar{h}$ spots always have the greatest separation due to twin domain orientation, while $h0h$ spots are not split at any value of θ. It follows that, while b is no longer parallel to b^*, it still lies in the plane containing b^* and the reciprocal lattice line $h0\bar{h}$, *i.e.* in the plane (101). Because of the twinning, its displacement within that plane will be towards $[10\bar{1}]$ in some domains, towards $[\bar{1}01]$ in others. The ac plane, common to the two twin components, is probably the composition plane; the b axis of each lies in a plane bisecting the *external* angle between the a and c axis, which is an acute angle.

It now becomes necessary to choose axes appropriate to phase N rather than phase P; though they still lie in pseudocubic directions, their senses are different. If we put $a_N = -a_P$, $c_N = c_P$, we have $\beta_N = \pi - \beta_P$ and $\alpha_N = \gamma_N$. Since $\beta_N < 90°$, it is natural to choose a sense for b that will make α_N and γ_N also $< 90°$.

Because of the impossibility, in general, of allocating a particular spot of a twin-related pair to a particular domain, it is only possible to measure the magnitude of the angles $\pi/2 - \alpha$, $\pi/2 - \beta$, and not their signs. The two magnitudes, however, are found to be equal at each temperature. Hence, with the above choice of axes,

$$\alpha_N = \beta_N = \gamma_N.$$

Using the earlier results that $a_N^* = b_N^* = c_N^*$, we have

$$a_N = b_N = c_N.$$

Dimensionally, therefore, the lattice has rhombohedral symmetry. This conclusion is not a consequence of our particular choice of axes of reference for phase N, but any other choice would have made it much harder to recognize.

It does not absolutely follow from the rhombohedral symmetry of the lattice parameters that the atomic positions, and therefore the structure as a whole, have also rhombohedral symmetry. This is, however, the most plausible working hypothesis at this stage, and we shall see that it is confirmed by the further evidence discussed in § 5.

4.2. *Lattice parameters of phase N*

Symmetrical back-reflexion photographs of crystals oscillating about $[001]_{pc}$ were used to obtain accurate θ values of about 10 independent reflexions. For a rhombohedral crystal we have

$$\frac{1}{a^*} = \frac{\lambda}{2 \sin \theta} [h^2+k^2+l^2+2 \cos \alpha^*(kl+lh+hk)]^{1/2}$$

where $\alpha^* > \pi/2$. Extrapolation against $\sin^2 \theta$ was carried out using Cohen's least-squares method. The relevant equation connecting the lattice parameters a^* and α^* and the systematic error parameter E with the observed θ value is

$$A(h^2+k^2+l^2)+B(kl+lh+hk)+E \sin^2 2\theta = \sin^2 \theta$$

where $A=\lambda^2 a^{*2}/4$, $B=\lambda^2 a^{*2} \cos \alpha^*/2$.

Independently, values of a^* were obtained from photographs such as 6(*b*) by measuring the difference in angle between 10,0,0, reflexions of phase *P* and *N*, whence knowing the value of a^* for phase *P* the value for phase *N* could be obtained. Furthermore, α^* could be measured directly from the separation of twin-related a^* axes of phase *N* on this photograph, which is equal to $2(\alpha^*-\pi/2)$. The values obtained from the different methods were the same within the estimated error.

Figs. 3 and 4 show the temperature dependence of the lattice parameters of phase *N* in comparison with those of phase *P* below room temperature. At -150 °C, the temperature at which intensities were measured, the values for the lattice parameters of phase *N* were measured as

$$1/a^* = a \sin^2 \alpha = 2(3{\cdot}9075 \pm 0{\cdot}0005) \text{ Å}$$
$$\alpha^* = 90°47' \pm 1'.$$

Hence $a = 2(3{\cdot}9083 \pm 0{\cdot}0005)$ Å, $\alpha = 89°13' \pm 1'$.

4.3. *The twin law*

Phase *N* always grows as a twin from either single or twinned crystals of phase *P*, both twin orientations having the same volume (see section on transformation rate). The symmetry of the proposed structure of phase *N* (see § 5) restricts the polarization direction to $[111]_{pc}$. However, the effects of the twinning will modify the resultant macroscopic polarization scheme. The twin laws consistent with the X-ray diffraction patterns are either a diad down [010], or a mirror plane (010). The mirror plane would result in head-to-head arrangement of the polarization vector, while the diad law gives a head-to-tail arrangement and is therefore the more likely of the two. The net polarization of a crystal twinned by a diad down [010] and made up of equal volumes of the two orientations lies along [010], with no resultant moment in directions perpendicular to this. This net polarization scheme agrees with what was found by Cross & Nicholson (1955), the polarization along [010] having the property of allowing reversal by an applied field.

5. Structure of phase *N*: preliminary considerations

5.1. *Symmetry and space group*

It was shown in § 4.1 that the lattice is dimensionally rhombohedral, and if pseudocubic axes are used it is face-centred. Moreover, all reflexions with *h*,*k*,*l*, odd are extremely weak.

There are in addition systematic absences for *hhl* reflexions with *l* odd.

The usual test for point-group symmetry, based on equality of intensities, cannot easily be applied. Reflexions of any set which would have been symmetry-equivalent in the aristotype are, experimentally, so nearly equal that differences due to twinning could mask any possible systematic differences due to structure; the weak difference reflexions are all so nearly zero that the same difficulty arises.

It is however possible to show that the array of niobium atoms is strictly rhombohedral. The scattered intensity is mainly determined by the niobium array, particularly at large scattering angles. If we take the origin at one of the two niobium atoms not related by face-centring vectors, the other is at $\frac{1}{2}+x, \frac{1}{2}+y, \frac{1}{2}+z$, where x,y,z are small. The geometrical structure factor for their contribution to the difference reflexions (those with h,k,l odd) may be written

$$F(\text{Nb}) = 4[1-\exp 2\pi i(hx+ky+lz)] . \qquad (2)$$

If any of the x,y,z were non-zero, then for large h, k or l the exponential term would differ appreciably from unity. This would result in a niobium contribution to all odd reflexions, increasing with increasing θ. However, the magnitude of the measured structure factors shows no such increase (see section on structure refinement). Hence we may conclude that the x,y,z of (2) are all zero, *i.e.* that the second Nb is exactly at $\frac{1}{2},\frac{1}{2},\frac{1}{2}$ relative to the first.

It follows that the niobium array is primitive with half the repeat distance of the structure as a whole in each direction, and hence that the array is strictly rhombohedral.

Since the lattice parameters, the niobium array, and the set of systematic absences are all consistent with rhombohedral symmetry, and there is no obvious departure from it in the intensity distribution, we may assume that it is correct.

Discussion of the space group is easier if we use rhombohedral axes of reference along the edges of the primitive rhombohedral (for which $\alpha \sim 60°$); this contains 2 formula units, and its relationship to the pseudocubic rhombohedron is shown in Fig. 7(*a*). The transformation is as follows:

$$a_r = \tfrac{1}{2}a_{pc} + \tfrac{1}{2}b_{pc}$$
$$b_r = \tfrac{1}{2}b_{pc} + \tfrac{1}{2}c_{pc}$$
$$c_r = \tfrac{1}{2}c_{pc} + \tfrac{1}{2}a_{pc} .$$

Using the same matrix for transformation of indices, the observed rule of systematic absences of *hhl* reflexions can be shown to keep its formulation un-

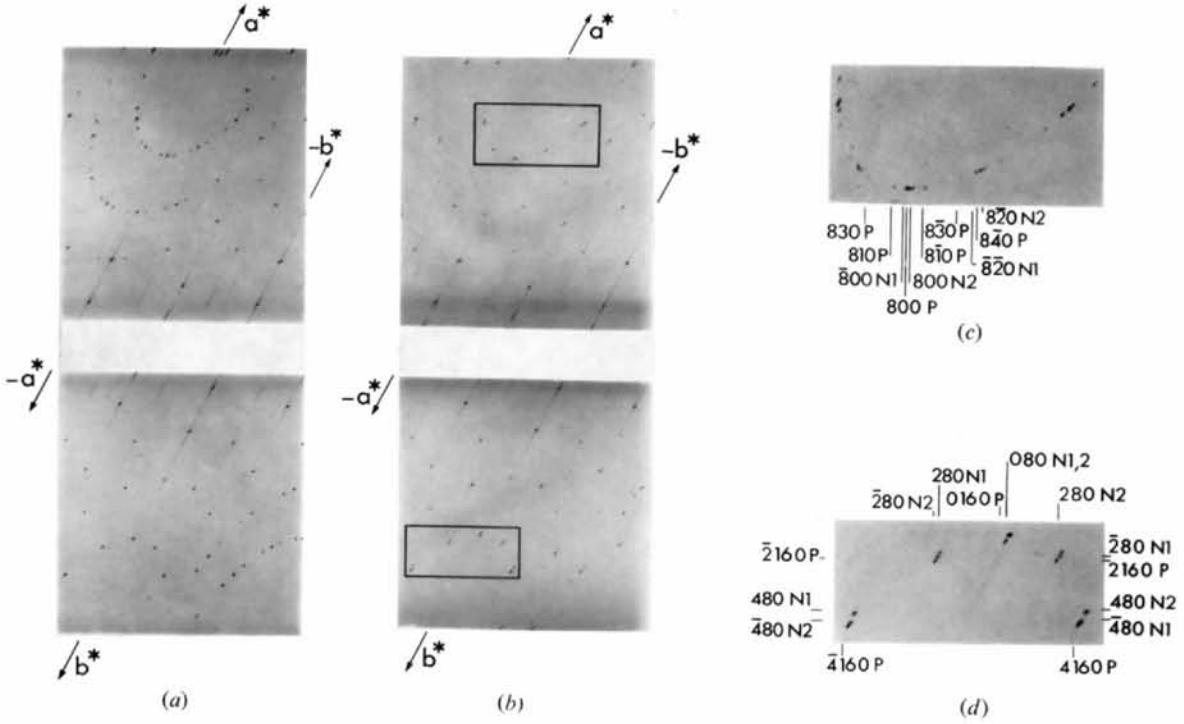

Fig. 6. Weissenberg photographs of $(hk0)_{pc}$ layer of a single crystal of phase *P*, (*a*) at room temperature, (*b*) at −110°C after previous cooling to −140°C for 15 min; (*c*) and (*d*), enlargements of parts of (*b*) shown in boxes. The $\alpha_1\alpha_2$ doublets are clearly resolved for the 480 complexes, and just distinguishable at lower θ-values.

[*To face p.* 2176

changed; it is then recognizable as the condition for the presence of a *c* glide plane. Taken in conjunction with the fact that, since the crystal is ferroelectric, its space group must be polar, the systematic absences fix the space group unambiguously as *R*3*c*.

Even without knowledge of the systematic absences, one might have expected *R*3*c* to be more likely than *R*3 or *R*3*m* (the other rhombohedral polar space groups), because in them the two niobium atoms would be independent, and an exact separation of $\frac{1}{2},\frac{1}{2},\frac{1}{2}$ would be fortuitous.

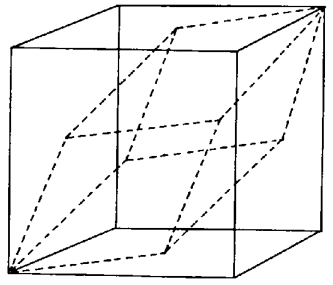

(*a*)

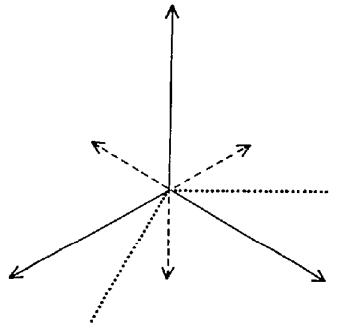

(*b*)

Fig. 7. (*a*) Perspective diagram showing relation of primitive rhombohedral cell and pseudocubic cell. (*b*) Projection down triad axis, showing relation of axes of pseudocubic cell (full lines), primitive rhombohedral cell (dashed lines) and hexagonal cell (dotted lines). The axes ending in arrows point upwards from the plane of projection.

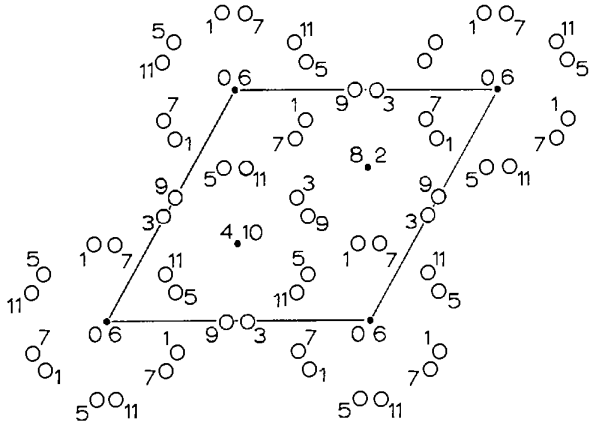

Fig. 8. Projection of atoms of NbO_3 framework down the triad axis. The base of the hexagonal unit cell is shown by full lines, O atoms by open circles. The numbers mark exact heights of O atoms and approximate heights of Nb atoms as multiples of $c_H/12$. Na atoms (not shown) project on top of Nb atoms, at a height difference of approximately $3c_H/12$.

5.2. *The trial model*

It is generally easier to visualize a rhombohedral structure using hexagonal axes of reference. We use the following transformation to obtain a unit cell containing 6 formula units:

$$a_h=\tfrac{1}{2}a_{pc}-\tfrac{1}{2}c_{pc}$$
$$b_h=-\tfrac{1}{2}a_{pc}+\tfrac{1}{2}b_{pc}$$
$$c_h=a_{pc}+b_{pc}+c_{pc}\,.$$

This is shown in Fig. 7(*b*). A schematic projection of $NaNbO_3$ using these axes of reference is given in Fig. 8. It can be seen to be isomorphous with $LiNbO_3$ (Abrahams, Reddy & Bernstein, 1966; Megaw, 1968).

Sodium and nobium atoms are placed in special positions 6(*a*) at $0,0,s$ and $0,0,t$ respectively, and oxygen atoms in general positions 18(*b*), at x_o,y_o,z_o. The origin is most conveniently chosen midway between layers of oxygens, making $z_o=1/12$. From the resemblance to the aristotype we then notice that s is nearly $\frac{1}{4}$, t is nearly zero, and the oxygen position may be written $\frac{1}{6}-2e-2d$, $\frac{1}{3}-4d$, $\frac{1}{12}$, where e and d are small. In the aristotype, where e and d are zero, all octahedra are parallel. If e is small and d is zero, the octahedra are rotated (or 'tilted') about the triad axis, but remain undistorted, except for a possible elongation or flattening down the triad axis. The tilt angle, ω, is given by

$$\tan\omega=4\sqrt{3}e\,.$$

If d is not zero, a distortion of the octahedron which makes the upper and lower faces unequal in size is permitted, as in $LiNbO_3$.

Though the structure is strictly isomorphous with $LiNbO_3$, it is not convenient to use the same hexagonal axes of references for the two structures, since $LiNbO_3$ is most conveniently described in terms of departure from ideal hexagonal closepacking, $NaNbO_3$ in terms of departure from ideal perovskite. The displacement parameter of oxygen, which is (for small tilts) proportional to the tilt angle is measured from axes which are 30° apart in the two cases. We prefer to return to the pseudocubic axes of reference for describing refinement of the structure, leaving comparisons till later. On these axes, the atomic positions are

Na: (s,s,s) with $s\sim\frac{1}{4}$
Nb: (t,t,t) with $t\sim 0$
O: $(-e+d,\frac{1}{4}-2d,e+d)$

The displacement parameters e and d have numerically the same values for both sets of axes. To fix the sense

of the [111] direction, we specify that t shall have a positive sign.

Trial values of the parameters were chosen as follows (Model I). For Nb, the components of displacement along the three pseudocubic axes were assumed to have the same value, 0·10 Å, as the components along two cubic axes in phase *P*. For Na, the displacement was assumed to be roughly twice that of Nb; this is in accordance with a general rule for rhombohedrally distorted perovskites, for which evidence has been cited by Michel, Moreau, Achenbach, Gerson & James (1969). For O, it was assumed that the octahedra were centrosymmetric, and that they were rotated by about 5° from their ideal-perovskite configuration. This gives the following set of trial parameters:

$$s=\tfrac{1}{4}+0{\cdot}026=0{\cdot}276\,,$$
$$t=0{\cdot}0125\,,$$
$$e=(\sqrt{3}/12)\tan\omega=0{\cdot}0536\,,$$
$$d=0\,.$$

5.3. *Predictions from lattice parameters*

It would in fact have been possible to predict the character of the octahedral framework and the magnitude of the tilt, simply from a knowledge of the lattice parameters of the pseudocubic lattice and the assumption of regular octahedra. If we write $\alpha=\pi/2-2\varepsilon$, it is easy to show that the axial ratio for hexagonal axes of reference is $c_H/a_H=\sqrt{6}(1+3\varepsilon)$, where the approximations used introduce an error of less than 1 % in the difference from unity of the factor in the bracket. Starting with an ideal cubic structure of regular octahedra and allowing them to tilt about the triad axes, we decrease the parameter a_H by a factor $\cos\omega$, while keeping c_H unchanged. Hence

$$1/\cos\omega=1+3\varepsilon$$

or

$$\tfrac{1}{2}\omega^2=3\varepsilon=3(\pi/2-\alpha).$$

This predicts a value of ω of $11\frac{1}{2}°$ – not far from the value actually obtained as a result of refinement (*cf.* § 6).

6. Structure of refinement of phase *N*

6.1. *Initial postulates*

Intensities from *hk*0, *hk*1, and *hk*2 pseudocubic layers collected at −150 °C were used in the structure refinement.

For the Fourier refinement, the atomic scattering factors adopted were those of Cromer & Waber (1965)

Table 1. *Observed and scaled calculated intensities for hk*1 *layer of phase N*

			Calculated intensity										Observed intensity
Angle ω			5·00		7·50		10·00		12·50		15·00		
Scale factor			2·00		1·03		0·72		0·60		0·57		
h	*k*	*l*											
3	$\bar{1}$	1	13·4		15·3		18·5		23·2		30 2		12
5	$\bar{1}$	1	5 8		6·1		6·7		7·3		8·0		6
7	$\bar{1}$	1	9·2		9·5		9·9		10·3		10·3		12
7	1	$\bar{1}$	9·2		9·5		9·9		10·3		10·3		9
9	$\bar{1}$	1	4·4		4·0		3·3		2·4		1·2		3
9	1	$\bar{1}$	4·4		4·0		3·3		2·4		1·2		3
7	$\bar{3}$	1	1·6	3·6	1·4	3·6	1·2	3·5	0·7	3·3	0·3	3·1	3
7	3	1	2·0		2·2		2·3		2·6		2·8		
$\bar{9}$	3	1	8·2	9·2	6·9	7·7	5·3	5·9	3·3	3·7	1·5	1·7	6
9	3	$\bar{1}$	1·0		0·8		0·6		0·4		0·2		
1	5	$\bar{1}$	5·8	11·6	6·1	12·2	6·7	13·4	7·3	14·6	8·0	16	15
$\bar{1}$	5	1	5·8		6·1		6·7		7·3		8·0		
3	5	$\bar{1}$	4·2	4·2	4·4	4·5	4·8	5·0	5·3	6·0	5·8	7·4	~1
$\bar{3}$	5	1	0		0·1		0·2		0·7		1·6		
7	$\bar{5}$	1	11·6		10·6		9·3		7·5		5·4		9
7	5	1	1·6		1·6		1·7		1·9		2·2		3
1	7	$\bar{1}$	9·2	18·4	9·5	19	9·9	19·8	10·3	20·6	10·3	20·6	24
$\bar{1}$	7	1	9·2		9·5		9·9		10·3		10·3		
3	7	$\bar{1}$	0	1·6	0	1·4	0·1	1·3	0·3	1·0	0·8	1·1	~1
$\bar{3}$	7	1	1·6		1·4		1·2		0·7		0·3		
5	7	$\bar{1}$	5·8		6·0		6·3		6·5		6·5		9
$\bar{5}$	7	1	10·6		10·6		9·0		7·5		5·4		12
1	9	$\bar{1}$	4·4	8·8	4·0	8·0	3·3	6·6	2·3	4·6	1·2	2·4	6
$\bar{1}$	9	1	4·4		4·0		3·3		2·3		1·2		
3	9	$\bar{1}$	1·0		0·8		0·6		0·4		0·2		~1
$\bar{3}$	9	1	0·0		0·1		0·4		1·0		1·9		0
	R_I %		26·2		23·8		22·4		28·7		44·4		
Excluding $3\bar{1}1$													
Scale factor			2·02		1·06		0·76		0·66		0·67		
	R_I %		26·4		24·2		18·6		21·2		35·0		

for Na^+, Nb^{3+}, and O^-;* for the least-squares refinement, they were those of Forsyth & Wells (1959).

An overall temperature factor was obtained from a plot of $\ln(F_o/F_c)$ *versus* $(\sin^2\theta)/\lambda^2$ for the $hk0$ layer, F_c being derived from the parameters of Model I. This gave $B=0{\cdot}58$ Å^2 for the intensities collected at -150°C. A similar plot for those collected at -110°C gave $B=0{\cdot}72$ Å^2.

6.2. *Use of hk*1 *layer*

Attention was first given to the $hk1$ intensities, to which, for this space group, only the oxygen atoms can contribute. All the 19 independent reflexions measured were extremely weak. They fell into two categories; those reflexions for which adjacent twin-related spots could be resolved were labelled category 1, while for category 2, the measured intensity was the sum of the two twin-related spots, namely $[I(hk1)+I(\bar{h}k\bar{1})]$. For cases where one of these was a systematic absence, the reflexion was placed in category 1.

A number of models were investigated, differing only in ω, the angle of rotation (or tilt) of the octahedron, which was given values in the range from 0 to 15° – a range which includes, though it does not restrict itself to, the value predicted from the lattice parameters. The distortion parameter d was zero throughout. The isotropic temperature factor was set at 0·6 Å^2. The calculated intensities were scaled to the observed intensities by equating $\sum I_c$ and $\sum I_o$ for each ω. Table 1 compares the five sets of I(calc) with the observed intensities. The R index, R_I, is defined as $\sum|K_jI_{cj}-I_o|/\sum I_o$ where K is the scale factor, the subscript j indicates the model, and the summation is over all the reflexions listed. It indicates that the best agreement is for ω close to 10°. However the R_I values are rather heavily weighted by one near-in reflexion $3\bar{1}1$, for which I_c is particularly sensitive to ω, and always greater than I_o. As a check, the calculation was therefore repeated with this reflexion omitted, with results shown in the lowest line of the table, again giving a minimum close to 10°. Graphical interpolation suggests a best value of $\omega=10{\cdot}8$°, with estimated limits of error of about 1·5°. This corresponds to $e=0{\cdot}028\pm0{\cdot}004$.

6.3. *Fourier refinement of hk*0

For Fourier refinement of the $hk0$ data, a new and simpler initial model was assumed (Model 2), with no deviations from ideal perovskite except the Nb displacement. This model (Table 2, column 2) gave a very reasonable R index of 10·31% indicating the dominance of the Nb contribution to the structure factors, yet the F_{obs} map [Fig. 9(*a*)] showed significant features pointing to the true structure. The oxygen peaks were elongated in a way consistent with rotation of the octahedra about the triad, and the Na peak was elongated along the face diagonal of the projection corresponding to the triad axis. Fig. 9(*b*) shows the contribution of the oxygen atoms by themselves at this stage; it is a difference map in which F_{calc} uses only the contributions of Nb atoms with $t=0{\cdot}0125$ and undisplaced Na atoms. Further refinement by difference syntheses gave the parameters listed in Table 2, column 3.

The origin of the unit cell and the sense of the axes were determined by the position of the heavy Nb atom and the condition that t should be positive. This means that the sign of $|s-t-\frac{1}{4}|$, whose magnitude is close to zero, has to be determined from the refinement. It was found that refinement only proceeded satisfactorily when it was given a positive trial value; if it was set negative, further cycles brought it back to zero and then refinement stopped. The zero value corresponds to a centrosymmetric array of sodium and niobiums, which is unable to refine further. With a positive initial value, the final value remained positive, but was dependent to some extent on the isotropic temperature

* The choice is based on an arbitrary assumption of 'half-ionized atoms' for the framework. In practice, for the accuracy of the present work, it makes little difference whether ionic or atomic f-curves are used. The different choices for the two techniques were dictated by the computing facilities available when the work was being done.

Table 2. *Parameters obtained during refinement of phase N*

		1 Trial model (I)	2 Trial model (2)	3 Fourier refinement of $hk0$	4 L.S. refinement of $hk0$ and $hk2$	5 Final values
Na, s	0·276		0·25	0·272	$0{\cdot}271_7\pm0{\cdot}008$	0·272
B(Na) Å^2	0·0		0·6	1·0	1·0 (Fixed)	1·0
Nb, t	0·0125	$B_o(-150°C)\sim0{\cdot}58$	0·0125	0·013	$0{\cdot}016_5\pm0{\cdot}003$	0·0165
B(Nb) Å^2	0·0	$B_o(-110°C)\sim0{\cdot}72$	0·6	0·6	$0{\cdot}66\ \pm0{\cdot}2$	0·66
0, e	0·0134		0·0	0·033	$0{\cdot}033_4\pm0{\cdot}004$	0·031
B(0) Å^2	0·0		0·6	0·6	0·6 (Fixed)	0·6
R index			10·31%	8·37%	7·89%	

Correlation matrix for column 4 parameters

	s	t	B(Nb)	e	Scale factor
s	1·00	0·54	0·22	−0·03	0·20
t		1·00	0·02	−0·13	0·00
B(Nb)			1·00	0·18	0·82
e				1·00	0·26
Scale factor					1·00

factor of Na. In the refinement, the oxygen parameter e was almost independent of s and t, as we should expect from the fact that their displacements are wholly in a plane normal to the displacements of the cations.

6.4. *Final refinement*

For the final stage, $hk2$ intensities were scaled to those of $hk0$, and used together with them for least-squares refinement. At first each atom was given an isotropic temperature factor, while d was kept zero. The values obtained for B(Na) and B(O) were physically ridiculous; hence these parameters were fixed at 1·0 Å^2 and 0·6 Å^2 respectively (values suggested by the Fourier refinement and close to those found in phase P). Refinement thereafter led to the final parameters given in Table 2, column 4. As a check, another refinement was carried out with the same initial parameters except that B(Na) was set at 1·5 Å^2; the differences in the final parameters were much less than their standard deviations, but the R index increased to 8·10%.

Attempts at refinement with a non-zero value of d proved unsuccessful, with the R index increasing. No attempt to refine anisotropic temperature factors was made.

The parameters finally adopted are given in Table 2, column 5. All are identical with those found in the least-squares refinement of $hk0$ and $hk2$ except for the oxygen position parameter e, where a mean has been taken between those from $hk0$ and $hk2$ on the one hand, $hk1$ on the other, since the two independent calculations have about the same accuracy. Comparison of F_o and F_c in Table 3, however, uses the parameters of Table 2, column 4.

7. Description of the structure

7.1. *Interatomic distances and deviations from ideal perovskite configuration*

The structure belongs to the perovskite family; we have to record how it differs from ideal perovskite in respect of the shape and orientations of the O_6 octahedron, the placing of Nb within it, and the environment provided for Na.

Bond lengths and octahedron edges are given in Table 4; some of the corresponding lengths for phase P and for other niobates at room temperature are included for comparison.

The Nb atoms are displaced from the geometrical centres of their octahedron by about 0·23 Å; all displacements are in the same direction, along the triad axis. There are thus three short and three long Nb–O bonds to each Nb, and one short and one long one to each O.

In spite of this off-centring of Nb, the O_6 octahedra are very nearly regular, as can be seen from the equality of the O–O edges within experimental error. It is this regularity which made possible the quantitative arguments of § 5.3.

Alternate octahedra are tilted in opposite directions about the triad axis by about 12°. This is a large effect; it implies that the oxygen array is not far from midway between that of ideal perovskite and ideal hexagonal close packing (for which the angle would be 30°).

The Na displacements, like the Nb displacements, are all parallel to the triad axis and in the same direction, but the Na displacements are larger, as follows

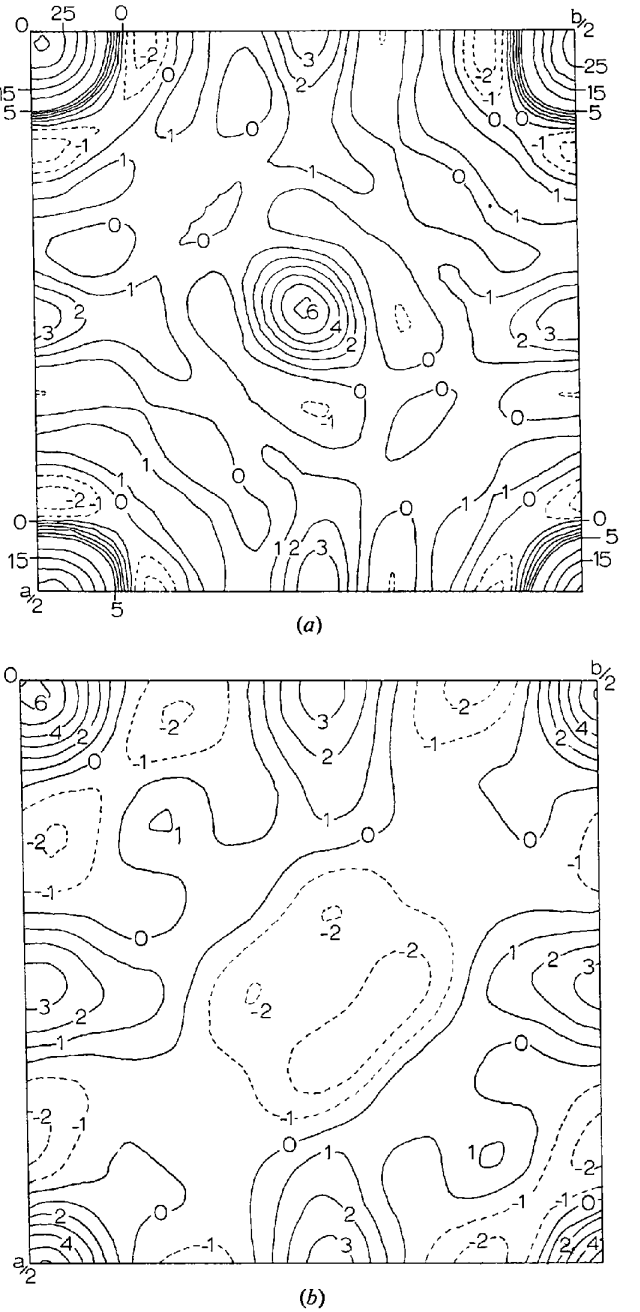

Fig. 9. (*a*) F_{obs} map for model 2, (*b*) difference map showing oxygen atoms only, with F_{calc} terms derived from a model containing only Nb and Na atoms in the positions of model 2. Contour intervals are at 1e Å^{-2} up to 5e Å^{-2} and thereafter at intervals of 5e Å^{-2}.

Table 3. *Scaled observed and calculated* structure factors for phase N*

h	k	l	F_{obs}	$\lvert F_{calc}\rvert$
0	0	0		760
2	0	0	302	318
4	0	0	394	454
6	0	0	155	168
8	0	0	217	221
$\bar{8}$	2	0	146	151
$\bar{6}$	2	0	228	231
$\bar{4}$	2	0	253	228
$\bar{2}$	2	0	331	339
2	2	0	358	365
4	2	0	268	250
6	2	0	241	254
8	2	0	160	161
$\bar{8}$	4	0	187	181
$\bar{6}$	4	0	155	137
$\bar{4}$	4	0	358	324
4	4	0	341	339
6	4	0	183	167
8	4	0	192	193
$\bar{6}$	6	0	214	171
6	6	0	202	200
8	6	0	92	130
$\bar{2}$	2	2	103	114
2	2	2	131	131
4	2	2	348	301
6	2	2	119	143
8	2	2	168	200
$\bar{6}$	4	2	259	214
$\bar{2}$	4	2	346	300
4	4	2	196	195
6	4	2	197	221
8	4	2	126	138
$\bar{6}$	6	2	150	141
$\bar{4}$	6	2	243	242
$\bar{2}$	6	2	125	141
6	6	2	132	139
$\bar{2}$	8	2	197	208

$F_c(000)$ is ten times the number of electrons associated with one formula unit.

* Using parameters of Table 2, column 4.

directly from the experimental observation that $s-t>\frac{1}{4}$.

The environment of Na, shown in Fig. 10, is irregular and unusual. This is not immediately obvious from the Na–O distances given in Table 4, according to which Na has six nearest neighbours at distances nearly equal to the sum of the ionic radii; but in Fig. 10(*a*), where they are marked by circles with inscribed crosses, and in Fig. 10(*b*), where they alone are included, their unbalanced spatial arrangement can be seen. The figure formed is not an octahedron; it can best be described as a distorted trigonal prism, in which one triangular face has been enlarged and twisted through an angle relative to the other. The six other oxygen atoms of the original twelve are all more distant. The six short edges of the prism – three horizontal edges in one triangular face, and three sloping edges joining it to the other face – are all shared with NbO_6 octahedra; in the other three edges, of the second triangular face, the oxygen atoms are not really in contact. We discuss this further in the next section.

7.2. *Comparison with* $KNbO_3$ *and* $LiNbO_3$

The low-temperature form of $KNbO_3$, occurring below about -50 °C, resembles phase *N* of $NaNbO_3$ in being rhombohedral, and in having its Nb atoms all displaced in the same direction along the trial axis (though the magnitude of the displacement has not been determined). It differs, however, in having no tilts; all its octahedra are oriented parallel to one another.

There is a closer resemblance between $LiNbO_3$ and

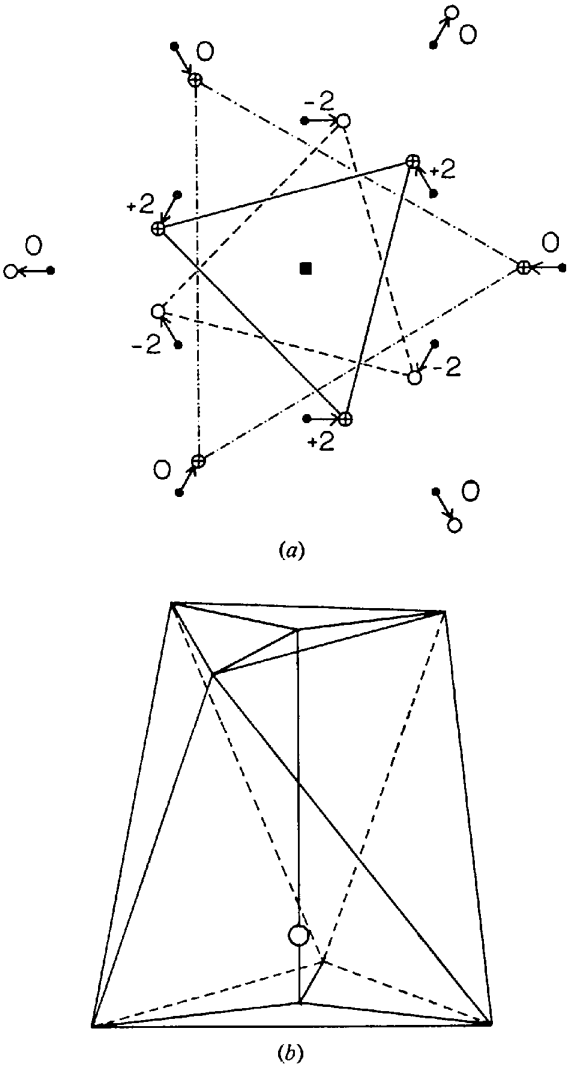

Fig. 10. Diagrams showing the Na environment. (*a*) Projection down the triad axis, with heights of oxygen atoms marked in units of $\frac{1}{12}$ the repeat distance; arrows show the displacements from positions in ideal perovskite and the six nearest neighbours of Na are distinguished by crossed circles. The Na atom (black square) is at height 0·26 units. The Nb atoms project at the same point as Na, at heights $-2{\cdot}80$ units, $+3{\cdot}20$ units. (*b*) Three-dimensional view, with the 6 nearest oxygens situated at the vertices of the polygon, and the sodium site shown by the open circle. The sodium is at a distance of 2·42 Å from the three oxygens forming the base and 2·56 Å from the remaining three.

phase *N* of $NaNbO_3$; they are in fact strictly isomorphous. In $LiNbO_3$ however, the independent deviations from ideal perovskite are larger: the Nb displacement is slightly increased; the tilt angle is 21°, approaching the value of 30° for hexagonal close packing; and the parameter v (analogous to d in phase *N*), which measures the distortion of the NbO_6 octahedron, is no longer zero. Most noticeable, however, is the difference between the environments of Na and Li. In both structures, the same six oxygen atoms are the nearest neighbours, but in $LiNbO_3$ they form a distorted octahedron instead of the distorted trigonal prism of $NaNbO_3$.

We can see the reason for the magnitude of the tilt, and the character of the *A*-cation environment, by considering the *A*-cation size. We postulate that tilts will be about the triad axis of the ideal structure. In $KNbO_3$ the K atom can touch twelve neighbours; indeed, the fact that the average O–O octahedron edge is rather larger in this than in the other structures of Table 4 suggests that K is large enough to push the oxygen atoms apart. We now consider an imaginary *A*-cation of gradually shrinking radius. The twelve original neighbours may be divided [as in Fig. 10(*a*)] into a set of six in the plane perpendicular to the triad axis and two sets of three above and below it, forming faces of NbO_6 octahedra. As *A* decreases in size, it moves up along the triad to keep contact with the three atoms above it, and the octahedra tilt about the triad in such a way as to allow alternate atoms of the set of six to move in and remain in contact with *A*; all the other original neighbours are further away. Of the six remaining neighbours, the three below *A* are at first still rather remote from each other, and unsymmetrically related to the first; this gives *A* a somewhat unbalanced environment. As the shrinkage continues, however, they approach each other more closely, and at the same time the first set of three rotates in its own plane, leading to the formation of a distorted octahedron. Finally when the size of *A* equals that of Nb, the oxygen atoms are in hexagonal close packing and the environment of *A* is a regular octahedron like that of Nb. The actual structures of $NaNbO_3$ (*N*) and $LiNbO_3$ correspond to two stages in this imaginary process: $NaNbO_3$ (*N*) to an intermediate stage, and $LiNbO_3$ to a later stage in which the environment is a recognisable though distorted octahedron.

Up to this point, we have assumed the NbO_6 octahedron to remain regular, unaffected by the *A* cation. In fact, however, we should expect the closer approach of *A* to one face to shorten the edges of that face, bringing about the distortion described by the parameter *d*. In $NaNbO_3$, the effect is not large enough to be detectable; in $LiNbO_3$, with its bigger Li displacement from the original 12-coordinated site, the observation agrees with expectation.

Table 4. *Interatomic distances* (Å) *in* $NaNbO_3$ *phase N and other niobates*

	1 $NaNbO_3$(*N*)	2 $NaNbO_3$(*P*)	3 $LiNbO_3$	4 $KNbO_3$ (orthorhombic)
Nb displacement	0·23	0·13	0·26	0·20
Nb–O	1·862 (2) [3] 2·122 (3) [3]	1·903 [2*m*] 1·974 [2*m*] 2·080 [2*m*]	1·889 [3] 2·112 [3]	1·863 [2] 1·991 [2] 2·180 [2]
A–O	2·42 (3) [3] 2·56 (8) [3] 3·05 (10) [3] 3·10 (3) [3]	(1) 2·421 [3*m*] 2·785 [6*m*] 3·088 [3*m*] (2) 2·440 [4*m*] 2·699 [4*m*] 3·140 [4*m*]	2·068 [3] 2·238 [3]	2·792 [4] 2·854 [4*m*] 2·873 [4]
O–O	2·803 (8) [3] 2·806 (11) [3] 2·804 [6*m*]	2·795 [4*m*] 2·798 [4*m*] 2·814 [4*m*] 2·802 [12*m*]	2·719 [3] 2·801 [3] 2·840 [3] 2·879 [3] 2·810 [12*m*]	2·780 [4*m*] 2·854 [4*m*] 2·884 [4*m*] 2·839 [12*m*]

Source of data:

Column 1: This work.
2: Sakowski-Cowley, Łukaszewicz & Megaw (1968).
3: Abrahams, Reddy & Bernstein (1966).
4: Katz & Megaw (1967).

[Note: The number enclosed in square brackets indicates the number of bonds of length stated; where it is followed by *m*, the bonds included are not all symmetry-equivalent, and the length given is their mean.]

8. Rate of $P \rightleftarrows N$ transformation

A large thermal hysteresis of about 100–150° was reported by Cross & Nicholson (1955) for the transition. We found that single-domain crystals of P transformed rapidly to twinned phase N for temperatures below about -130°C, and that the reverse transition was again rapid, occurring at about -50°C. These crystals always returned to single-domain crystals of phase P.

The large hysteresis is probably caused by the great structural change required at the transition, tending to make nucleation of the appearing phase difficult. Furthermore, rapid growth of the appearing phase would be the result of the fact that the interface between the nuclei and bulk must have a high energy.

Type-1 twinned crystals of phase P showed different behaviour. This type of twinning leaves b_o unique but a_o and c_o of adjacent domains approximately parallel. In reciprocal space this brings $h0l_{pc}$ and $\bar{h}0l_{pc}$ lattice points close together. The domain walls lie in $(100)_{pc}$ planes and are 'permissible walls' satisfying the criteria of Fousek & Janovec (1969), falling into their W_f category (*i.e.* the two domains are dimensionally matched at the boundary as indeed are the two orientations of phase N at their common $(010)_{pc}$ plane). However type-1 domains are no longer matched in phase N as Fig. 11 shows. Therefore the $P \rightarrow N$ transition in a crystal with type-1 twinning must be associated with considerable self-imposed stress tending to inhibit the transformation.

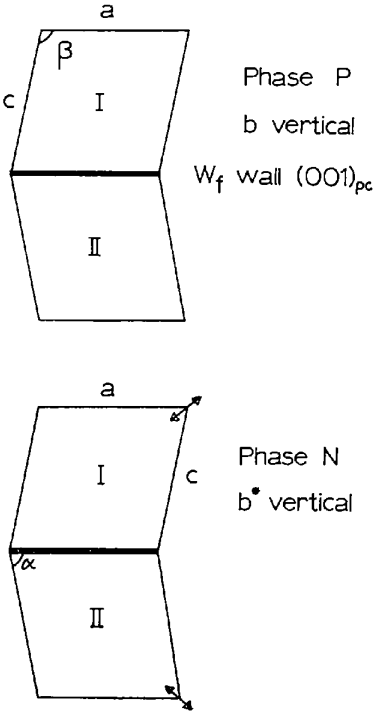

Fig. 11. Juxtaposition of domains in type-1 twinning in phases P and N. The heavy line marks the trace of the wall in the (010) plane; in phase P the plane of the wall is perpendicular to (010), but in phase N it is inclined at an oblique angle to it, in one of four possible orientations, since [010] has moved away from the vertical in one of the four directions indicated by the small arrows.

Fig. 12 shows eight oscillation photographs of a type-1 twinned crystal of phase P oscillated about [010]. The crystal was cooled to -165°C, held there for 15 min, and the left-hand photograph started. Only the zero-layer was recorded. After 30 min, the cassette was moved along, and the second exposure begun. This process was repeated to give the other photographs, each exposure separated by about 20 sec.

The phase P spots lie on the central straight line of each exposure; those included in the oscillation range have indices $h0l$ with $l=4$, and 10,0,0. Because of the twinning, they occur in pairs $h04/\bar{h}04$, except for $10,0,0/\bar{1}0,0,0$ which coincide. Each spot except 404 has satellite reflexions coming from the growing twinned-phase-N portions. The 404 spot of phase N is slightly displaced from that of phase P because of a small misfit of the lattices in the $(010)_{pc}$ plane.

In the first exposure, one orientation of twinned-phase-N has already appeared. We expect twin-related $h0l$ spots of N to have the same structure factor if we neglect anomalous dispersion; the observed equality of their intensities on the photograph indicates that the two twin components are of equal volume.

With successive exposures, a second orientation of twinned-phase-N appears, inclined at a small angle to the first, and its spots increase in intensity till they equal those of the first. Comparison of 10,0,0 complexes in the different exposures shows this effect clearly.

Similar series of photographs of the same crystal taken at warmer temperatures showed the transformation rate to be strongly temperature-dependent. 22 hr at -114°C were required for the intensity of the phase N spots to reach the level shown in the first photograph of Fig. 12, taken after 15 min at -165°C.

It is important to stress the fact that Cu $K\alpha$ radiation is strongly absorbed by $NaNbO_3$, so that any conclusions about the transformation rate deduced from the intensities are for the surface region only.

All type-1 twinned crystals of phase P returned to their original twinned state on the reverse $N \rightarrow P$ transition.

The other commonly occurring form of twinning in phase P is termed type II (LŁM, 1966). Here the b axes of adjacent domains are approximately perpendicular. The transition $P \rightarrow N$ is accompanied by an increase in b of approximately 1%.

In one crystal the type-II twinning disappeared after cooling the crystal to -150°C. In other crystals both twinned phase N and type-II twinned phase P coexisted.

9. Discussion

9.1. *Principles and their application*

The structure of $NaNbO_3(N)$ and the nature of the $N \rightarrow P$ transition can be understood in terms of cer-

tain empirical generalizations applicable to most distorted perovskites.

(1) There are two effects, independent in their origin, giving rise to distortions. These are the off-centring of the *B*-cation within the BO_6 group, and the tilting of octahedra, controlled by the size of the *A*-cation.

(2) The off-centring is an intrinsic property of the BO_6 group, though it may be modified by external effects of the structure into which the group is built. It is temperature dependent; the sequence with increasing temperature is 3-corner (triad axis), 2-corner (diad axis), 1-corner (tetrad axis) and zero (undisplaced), and the transition temperatures (except as modified by external effects) are characteristic of the group.

(3) The oxygen atom participates in either one short B–O bond and one long one, or in two medium length ones.

(4) The tilts are such as to provide an environment in which the *A*-cation has nearly equidistant oxygen neighbours holding it in position.

(5) Though independent in origin, the *B*-cation displacements and the tilts interact; in particular, the symmetry of the tilt system and the symmetry of the *B*-cation displacement influence one another.

When atoms such as Pb are present, which are known chemically to form covalent bonds, some further discussion is needed; but we shall not be concerned with them here.

With these ideas, the structure of $NaNbO_3(N)$ might have been predicted. At low temperatures we expect a triad-axis displacement of Nb, as in $KNbO_3$. Because of the short–long alternation at O, all Nb displacements must be in the same direction, again as in $KNbO_3$. The small size of Na requires some kind of tilt; because the Nb displacement is along the triad-axis, a triad-axis tilt is favoured, which has the effect described in § 7.2.

As we have seen, the environment of Na is unusual, and intuitively it seems likely to be unstable. We therefore expect to find the transition from triad-axis displacement to diad-axis displacement occurring at a rather lower temperature in $NaNbO_3$ than in $KNbO_3$, where the environment of K is not abnormal, and where we may take the transition temperature, $-50\,^{\circ}C$, as characteristic of the NbO_3 group.

In $LiNbO_3$, on the other hand, triad-axis displacement persists up to 1200 °C. Here, however, the Li environment is normal. It would seem that because a large triad-axis tilt is required to provide for Li, a triad-axis symmetry is favoured, and the triad-axis displacement of *B* is extended to a far higher temperature than would otherwise be possible.

Thus in both low-temperature $NaNbO_3$ and room-temperature $LiNbO_3$ there is a conflict between the local energy requirements of the *A* and *B* cation environments, but in $NaNbO_3$ it is the *B*-cation that determines the structure and imposes its symmetry on the other, in $LiNbO_3$ it is the *A*-cation.

There can, of course, be other factors contributing to the stability of the triad-axis displacement in $LiNbO_3$, for example, the electrostatic repulsion between Nb and Li. This illustrates an extension of a principle stated in a more restricted way by Baur (1972): that a structure tends to be stable if the *same* geometrical distortion helps to satisfy more than one *independent* requirement of local atomic environments.

Comparisons of $NaNbO_3$ phase *N* with other rhombohedral perovskites will be left to a separate paper.

9.2. *The $N \rightarrow P$ transition*

It is easiest to compare the different phases of $NaNbO_3$ if we think of displacements as made up of component displacements along the three tetrad axes of the original cube, and tilts as made up of component tilts about the same three axes.

At the $N \rightarrow P$ transition, one component of Nb displacement is lost. Empirically, we might expect a decrease of Nb displacement in the ratio $\sqrt{2}/\sqrt{3}$, which would give a value of 0·18 Å in phase *P*, instead of the observed 0·13 Å. The prediction does not allow for modification of the displacement by interaction with the rest of the structure; in room-temperature $KNbO_3$, with two components like $NaNbO_3$ (*P*), the displacement is 0·20 Å. Qualitatively, the idea holds good; quantitatively, it is only very rough. In what follows, we shall be concerned with the existence, sense, and symmetry relations of displacement components and tilt components, and not with their exact magnitudes.

In phase *N*, the trigonal symmetry – a consequence of the 3-corner displacement – requires the three components of tilt, like the three components of displacement, to be equal. In phase *P*, where one component of displacement has been lost, this symmetry requirement applies only to the other two, and the two tilt components about the same axes. The symmetry axis is now a face-diagonal of the $(010)_{pc}$ face. The tilt component about the $[010]_{pc}$ axis is now independent of the others.

The relative senses of the Nb displacements in different octahedra are not determined by the existence of the symmetry axis. The requirement of alternate short and long Nb–O bonds means that for phase *P*, within the $(010)_{pc}$ plane, they are all parallel, but their directions in successive planes are not specified by this, and we have to look for other reasons why they should be parallel or antiparallel.

The changes of tilt can be discussed in terms of Glazer's (1972) treatment. When the $[010]_{pc}$ tilt component is held equal to the others by a triad axis of the structure, it must change sign in successive $(010)_{pc}$ layers; the tilt system for phase is $a^-a^-a^-$. When it is independent, it may keep the same sign, and if it does so $(010)_{pc}$ becomes a mirror plane; the tilt system is then $a^-b^+a^-$.

It is simplest first to consider the transition $N \rightarrow Q$ (which has not been directly observed in this work).

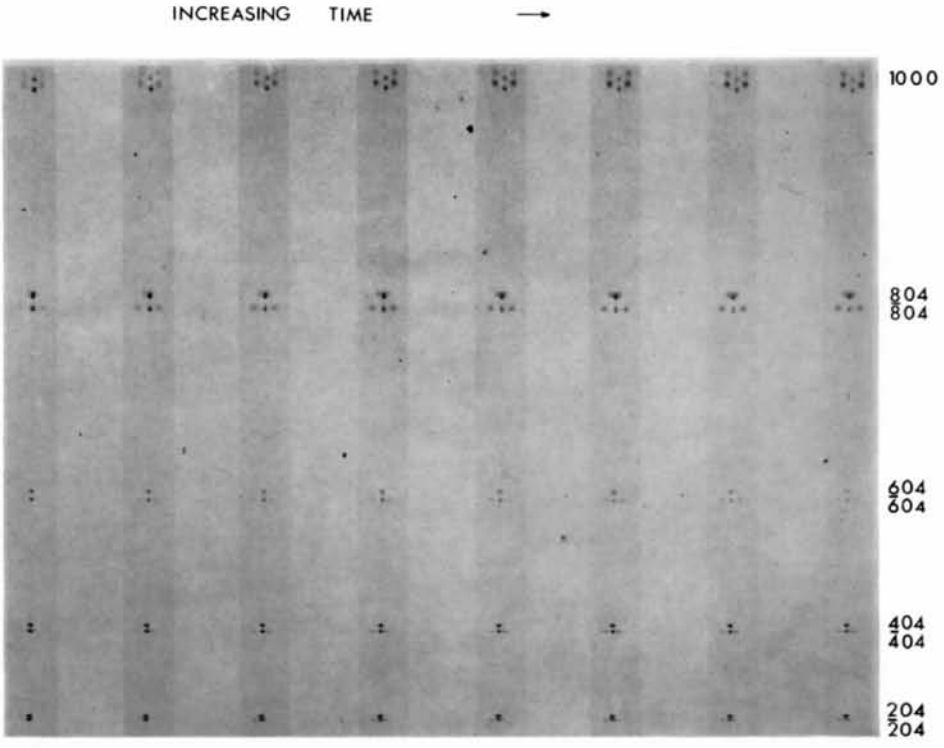

Fig. 12. Set of eight oscillation photographs, taken at equal time intervals of 30 min of a type-I twinned crystal held at −165 °C. The oscillation range was chosen to give a set of spots carrring useful information. Spots from both phase *P* and phase *N* occur in all photographs.

The structure of Q and its relation to $Na_{0.975}K_{0.025}NbO_3$ is discussed by Wells & Megaw (1961), Wood, Miller & Remeika (1962) and LŁM (1966). For Q alternate layers must change the sense of their $[010]_{pc}$ tilt, without changing the sense of their Nb displacement components. There are now mirror planes between all $(010)_{pc}$ layers, and the shape of the cavity available to Na has changed, giving a fairly regular 8-cornered environment. A disadvantage of the mirror-plane symmetry is that Nb displacements in successive layers are parallel, which is energetically unfavourable except in the presence of an electric field parallel to the displacement.

The transition $Q \rightarrow P$ requires further changes of sense. Alternate *pairs* of layers in Q reverse both the sense of their $[010]_{pc}$ tilt and the direction of their Nb displacement, keeping a mirror plane within each pair. Between pairs, the Na environment is less well balanced, but the electrostatic interaction is favourable.

Though this two-step process is the easiest way to describe the $N \rightarrow P$ transition, it is not necessarily the correct one. A one-step process would require the reversal of $[010]_{pc}$ tilts of pairs of $(010)_{pc}$ layers, accompanied by the reversal of Nb displacements in out-of-phase pairs of layers.

We can now understand the difficulty of achieving the $P \rightarrow N$ transition, and the consequent large thermal hysteresis. It is not the change of Nb displacement which is itself difficult. But, because of it, layers of octahedra have to rotate cooperatively relative to their neighbours, and produce a large change in the Na environment; instantaneously, there must be very large compressions of certain Na–O distances, giving rise to a large energy hump. Moreover, the final volume of P is appreciably smaller than that of N, because of the smaller volume associated with Na; hence there will be very large elastic stresses at domain boundaries in a twinned crystal, or if the crystal is clamped by its support.

9.3. *Other phases of* $NaNbO_3$

The sequence of transitions in $NaNbO_3$ can now be seen as a consequence of the interaction of Nb displacements and tilts about Na. Phase N is the simplest of the phases possessing Nb displacements; the displacements have three equal components, and the tilts also three components held equal by symmetry. In phases P and Q, there are two equal displacement components, two equal tilt components about the same axis, and one independent tilt component. In phase R there is one displacement component and three independent tilt components. The higher phases (Ahtee, Glazer & Megaw, 1972) have no Nb displacements; phase S retains three independent tilt components, phase T_1 has two, phase T_2, one. The disappearance of the two final tilt components can be correlated with one-phonon modes. At lower temperatures, when the tilts and displacements are coupled through the symmetry, the relations are more complex, but it is interesting to see how the continuity of the series can nevertheless be analysed in terms of the interactions and different temperature dependences of fairly simple geometrical factors.

We wish to acknowledge our indebtedness to the Science Research Council, both for its general support of the studies of which this work forms a part (H.D.M.), and for an individual grant to one of us (C.N.W.D.). We are grateful to Mr G. G. Yates of the Cavendish Laboratory for designing the electronics of the low-temperature apparatus.

References

ABRAHAMS, S. C., REDDY, J. M. & BERNSTEIN, J. L. (1966). *J. Phys. Chem. Solids*, **27**, 997–1012.
AHTEE, M., GLAZER, A. M. & MEGAW, H. D. (1972). *Phil. Mag.* (*Ser.* 8) **26**, 995–1014.
BAUR, W. H. (1972). *Amer. Min.* **57**, 709–731.
CROMER, D. T. & WABER, J. T. (1965). *Acta Cryst.* **18**, 104–109.
CROSS, L. E. & NICHOLSON, B. J. (1955), *Phil. Mag.* (*Ser.* 7) **46**, 453–466.
FORSYTH, J. B. & WELLS, M. (1959). *Acta Cryst.* **12**, 412–415.
FOUSEK, J. & JANOVEC, V. (1969). *J. Appl. Phys.* **40**, 135–142.
GLAZER, A. M. (1972). *Acta Cryst.* B**28**, 3384–3392.
KATZ, L. & MEGAW, H. D. (1967). *Acta Cryst.* **22**, 639–648.
LEFKOWITZ, I., ŁUKASCEWICZ, K. & MEGAW, H. D. (1966). *Acta Cryst.* **20**, 670–683.
MEGAW, H. D. (1957). *Ferroelectricity in Crystals*. London: Macmillan.
MEGAW, H. D. (1968). *Acta Cryst.* A**24**, 583–588.
MICHEL, C., MOREAU, J.-M., ACHENBACH, G., GERSON, R. & JAMES, W. J. (1969). *Solid State Commun.* **7**, 865–868.
PARRISH, W. (1960). *Acta Cryst.* **13**, 838–850.
SAKOWSKI-COWLEY, A. C., ŁUKASZEWICZ, K. & MEGAW, H. D. (1969). *Acta Cryst.* B**25**, 851–865.
SEARS, J. E. & TURNER, A. (1941). *J. Sci. Instrum.* **18**, 17–19.
WELLS, M. & MEGAW, H. D. (1961). *Proc. Phys. Soc.* **78**, 1258–1259.
WOOD, E. A., MILLER, R. C. & REMEIKA, J. P. (1962). *Acta Cryst.* **15**, 1273–1279.